Crater Formation on Electrodes during Charge Transfer with Aqueous Droplets or Solid Particles

E. S. Elton, E. R. Rosenberg, and W. D. Ristenpart

Crater Formation on Electrodes during Charge Transfer with Aqueous Droplets or Solid Particles

E. S. Elton,[1] E. R. Rosenberg,[1, *] and W. D. Ristenpart[1, †]

[1]*Department of Chemical Engineering, University of California Davis, Davis, CA 95616, USA.*

We report that metallic electrodes are physically pitted during charge transfer events with water droplets or other conductive objects moving in strong electric fields (>1 kV/cm). *Post situ* microscopic inspection of the electrode shows that an individual charge transfer event yields a crater approximately 1 to 3 microns wide, often with features similar to splash coronae. We interpret the crater formation in terms of localized melting of the electrode via resistive heating concurrent with dielectric breakdown through the surrounding insulating fluid. A scaling analysis indicates that the crater diameter scales as the inverse cube root of the melting point temperature T_m of the metal, in accord with measurements on several metals ($660°$C $\leq T_m \leq 3414°$C). The process of crater formation provides a possible explanation for the longstanding difficulty in quantitatively corroborating Maxwell's prediction for the amount of charge acquired by spheres contacting a planar electrode.

A water droplet or other conducting object, when immersed in an insulating fluid, acquires a charge when it contacts an electrode [1, 2]. Provided the electric field is strong enough, the conducting object will move away to the opposite electrode, acquire the opposite charge, and repeat the process, effectively bouncing back and forth between the electrodes [3–7]. Although this qualitative behavior has been well established, experimental measurements of the amount of charge transferred have been marked for decades by irreproducibility [8–11] and significant deviations [10–15] from the theoretical prediction first derived by Maxwell [1]. Experimental work indicates general agreement with the theory, but close examination of the data shows that the charge transferred to the same object from the same electrode can vary up to 200% [8–11]. Recent measurements with metal particles indicate that the particles received 34% less charge on average than predicted [11].

A key implicit assumption, dating back to Maxwell, has been that the electrode remains unaltered by the charging process. In this Letter we demonstrate that the electrode is physically pitted during charge transfer events with an individual water droplet or metallic sphere. We characterized a variety of different metal electrodes using optical, electron, and atomic force microscopy before and after water droplets or metallic spheres were electrically bounced on them. Although the electrodes appear unchanged to the naked eye, the microscopy reveals that the charge transfer events yield craters approximately 1 micron wide. A scaling analysis indicates that the crater diameter increases with the cube root of the ratio of the energy exchanged during charge transfer to the melting point of the metal, i.e., $d \sim (E/T_m)^{1/3}$, in accord with experimental measurements. Finally, we discuss how the process of crater formation helps explain longstanding irreproducibility in precise measurements of charge acquisition, as well as the practical implications for devices that use electric fields to manipulate charged objects [16–19].

The physical changes to the electrodes are readily produced using a pair of planar thin metal films (50 nm to 1 μm thick) each deposited on a glass slide using standard photolithographic techniques (Fig. 1 and Fig. S1 [20]). The electrodes are placed 8 mm apart inside a plastic cuvette, which contains either air or an insulating fluid (e.g. silicone oil) (Fig. 1(a)). To begin an experiment, a voltage between 1 and 10 kV is applied, and then either a 3.5 μL water droplet (Fig. 1(b)) or a 2.4 mm diameter metallic ball pendulum (Fig. 1(c)) is inserted. Upon

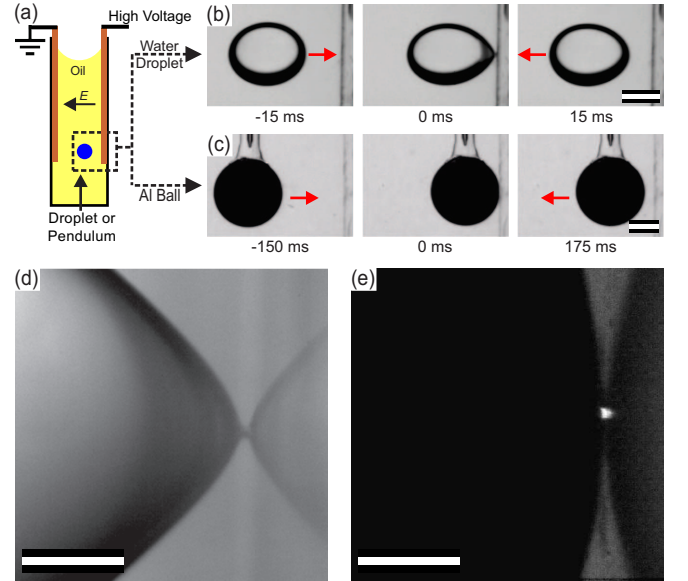FIG. 1. (a) Schematic of experimental setup. (b,c) Time lapse images of (b) a 3.5 μL pH 7 buffered water droplet and (c) a 2.4 mm aluminum ball pendulum approaching, contacting, and departing from an electrode in silicone oil. Arrows indicate direction of motion. (d,e) Higher magnification images of the contact between the electrode and (d) an aqueous droplet or (e) an aluminum ball. Reflection of droplet or ball is visible at right. A flash of light is visible in (e). Scale bars: (b,c) 1 mm, (d,e) 200 μm. See also movies S1-S4 [20].

contact with an electrode, the droplet or ball becomes charged and is repelled toward the opposite electrode, where the process repeats. Gravity causes droplets to sink as they bounce back and forth, but positive dielectrophoretic forces [21] near the bottom of the electrodes counteract gravity so that the droplets bounce laterally at an approximately constant vertical position. As the drop approaches the electrode, the electric stresses cause the drop to assume a conical shape known as a Taylor cone (Fig. 1(d)) [22, 23].

The droplet or ball is typically allowed to bounce back and forth for 30 minutes, representing hundreds to thousands of individual charge transfer events. Motion is recorded using high speed video, and the system electrical current is measured simultaneously with a high resolution electrometer. Depending on the applied field strength the metal balls bounce with a frequency of 1 to 8 Hz (1.6 to 13 cm/s), while water droplets transit at approximately 3 Hz (5 cm/s) in an applied potential of 3.3 kV. Analysis of the recorded video to determine the corresponding acquired charge (by balancing the electrostatic force versus the drag force) indicates that the metal ball typically receives about 70 pC to 250 pC of charge from either electrode depending on the applied field strength, while the droplet receives approximately 110 and 200 pC from the negatively and positively charged electrode respectively. The overall behavior of the droplets and metal balls, including the magnitude of charge acquired, is broadly consistent with previous studies [9, 14, 18, 19, 24].
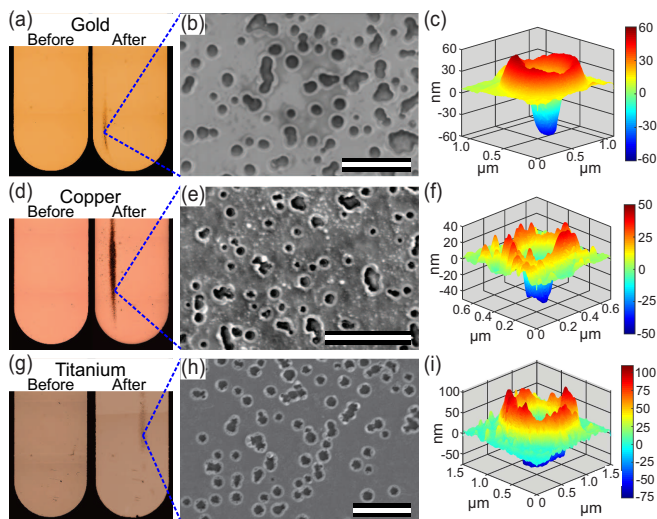

FIG. 2. Craters formed during charging of aqueous droplets on 50-nm thick gold, copper, or titanium electrodes, each 0.5 mm wide, in a 0.4 kV/mm electric field in silicone oil. (a,d,g) Representative reflection microscopy images of positively charged electrodes before and after a 3.5 μL droplet was electrically bounced on them. (b,e,h) Representative SEM images showing circular pits or craters. Scale bar: 5 μm. (c,f,i) Representative AFM images of individual craters. Heights are in nm, lateral dimensions are in μm.

Examination of 50-nm thick electrodes after electrically bouncing a water droplet reveals no changes visible to the naked eye. Microscopic inspection of the positively charged electrode, however, reveals significant changes (Fig. 2). Optical reflection microscopy (following thorough solvent rinses to remove oil) shows a darkened region in the approximate area where the aqueous droplet had repeatedly contacted (Fig. 2(a,d,g)); here a darker color indicates less reflected light. Optical transmission microscopy confirms that these regions allow light to pass through (Fig. S2 [20]). Control experiments with an applied field but without a bouncing droplet yield no changes to the electrode visible by microscopy, and experiments with systematically increased droplet bounce times (e.g., 60 or 90 minutes of bouncing) yield generally larger and more transparent regions on the electrode.

Higher resolution images of the electrode surface using scanning electron microscopy (SEM) reveal that the affected regions contain many hundreds to thousands of circular pits or craters (Fig. 2(b,e,h)). Larger pits appear to be composed of several superimposed individual circular pits, each approximately 0.5 microns in diameter. The surface elemental composition, as determined through energy dispersive spectroscopy (EDS), indicates that the center of each pit or crater contains relatively less of the electrode metal and more oxygen and silicon in a ratio similar to the uncoated glass substrate (Fig. S3 [20]). Together, the optical and electron microscopy observations are consistent with the interpretation that the metal film has been at least partially removed from the center of each pit.

Atomic force microscopy (AFM) measurements indicate that each pit is shaped like a crater, with a depression surrounded by a "rim" significantly higher than the surrounding electrode surface (Fig. 2(c,f,i)). The craters are approximately 50 nm deep, consistent with the EDS and transmission microscopy results indicating an uncovered glass substrate, while the surrounding rims rise approximately 50 to 200 nm above the surface of the film. Importantly, numerical integration of the AFM height data indicates that the volume enclosed in each crater rim is approximately equal to or exceeds the volume of each crater depression (see supplemental material for details [20]). This observation strongly suggests that the metal originally in the crater depression was simply displaced during the crater formation, rather than physically removed from the electrode surface.

Further experiments indicate that the crater formation is a robust consequence of charge transfer. Craters were observed on a wide variety of other metal types, including nickel, tungsten and aluminum. Local deformations produced by bouncing water droplets were also observed on the negatively charged electrodes, albeit with less dramatic morphology possibly resulting from the smaller amount of charge transferred (Fig. S4 [20]). Experiments with thicker metal films (1 μm instead of 50 nm) yielded
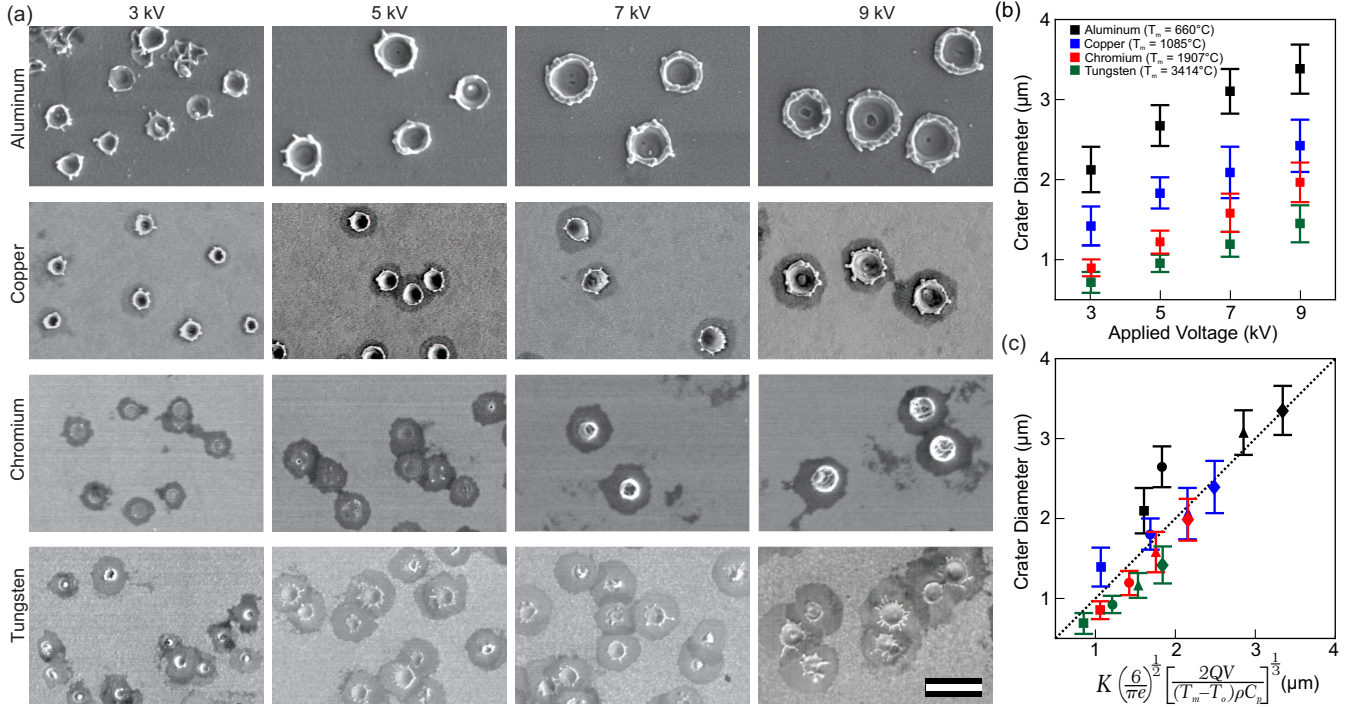
FIG. 3. Increase in crater size with applied voltage on various metals. (a) Representative SEM images of craters formed during the charging of a 2.4 mm diameter aluminum ball on 1-μm thick electrodes composed of aluminum, copper, chromium, or tungsten under different applied voltages. Scale bar: 5 μm. (b) Average crater diameter versus applied voltage for different metals. Each point is the average of 100-200 craters; error bars represent one standard deviation from the mean. (c) Average crater diameter versus scaling prediction (Eq. (1)) with dimensionless prefactor $K = 0.187$. The dashed line has slope equal to 1. Color codes same as in (b); marker shapes indicate the applied voltage (squares, 3 kV; circles, 5 kV; triangles, 7 kV; diamonds, 9 kV).

small changes to the surface of the electrode, suggesting that the crater formation is not a consequence of charge transfer through a thin electrode.

Most importantly, experiments with solid metal pendula yield craters extremely similar in nature to those created by the water droplets (Fig. 3). The average crater diameter depends on the type of metal used for the electrode, and increases with the applied potential (Fig. 3(b)). No statistically significant difference in crater size is found between the positively and negatively charged electrodes (Fig. S5 [20]). Experiments with metal pendula suspended in air also yield craters (Fig. S6 [20]), indicating that the crater formation does not require a liquid phase. Qualitatively similar craters were also observed to form on the metal pendulum (Fig. S7 [20]).

Why do the craters form? Several pieces of evidence point to transient melting of the metallic electrode as the underlying mechanism. First, there is no evidence of compositional changes to the electrode, merely displacement of the metal out of the crater depression and into the surrounding rim. Second, many of the craters exhibit splash-like features qualitatively similar to the corona observed in a liquid splash [25], as evidenced by the undulations in the rims that are generally directed ra-

dially outward from the crater center. This morphology would be consistent with melting of the metal concurrent with an outward transfer of momentum, followed by rapid cooling and re-solidification. It is not clear why this morphology is not observed for craters formed from the contact of a droplet and electrode; one possibility is that the smaller amount of molten material does not allow the metal to splash. Third, the crater size decreases with the melting point of the metal used for the electrode (cf. Fig. 3(b)). Aluminum (melting point 660°C) exhibits the largest diameters, while copper (melting point 1085°C), chromium (melting point 1907°C) and tungsten (melting point 3414°C) exhibit systematically smaller craters respectively. For a given amount of energy transferred, the molten area will be larger for a lower-melting-point material because less energy is required to raise the temperature to the melting point.

Although it might seem counterintuitive that the metal electrode could reach temperatures as high as 3414°C during close contact with a room temperature water droplet, a scaling analysis suggests that the energy exchanged during charge transfer is sufficient to melt regions similar in size to the observed craters. The heat released via Joule heating is proportional to the electrical power P integrated over time t_c during the charge trans-

fer, and can be estimated as $E \approx Pt \approx VIt_c$, where V is the applied voltage difference and I the current flowing between the electrode and droplet or ball. Recognizing that It_c is the amount of charge Q the droplet or ball acquires, the heat applied to the metal can be estimated as $E \approx QV$. The maximum diameter d_{max} that rises above a melting temperature T_m can be estimated from the transient heat equation with an instantaneous point source of magnitude QV, yielding the scaling estimate

$$d_{max} \approx K \left(\frac{6}{\pi e} \right)^{\frac{1}{2}} \left[\frac{2QV}{(T_m - T_o)\rho C_p} \right]^{\frac{1}{3}}, \qquad (1)$$

where T_o, ρ and C_p are the initial temperature, density and heat capacity of the electrode material (see supplemental material for derivation of Eq. (1) [20]). The charge Q is estimated by integrating the measured current between each charge transfer (cf. Fig. 4), leaving the dimensionless prefactor K as the only adjustable parameter. A plot of the observed crater diameters versus Eq. (1) yields excellent agreement (Fig. 3(c)). Importantly, linear regression yields a best fit value of $K = 0.187$, which suggests that the energy associated with charge transfer is more than sufficient to melt the metallic electrodes to the observed diameters. The theory discussed here neglects more complicated effects such as the heat of melting and the finite size and duration of the heat source, and assumes that all of the heat released enters the electrode. Nonetheless, the scaling analysis strongly suggests that the craters form through the transient melting of the electrode material.

If enough energy is transferred to melt the metal, what provides the radially directed outward momentum necessary for crater formation in the molten metal? Our high speed video observations provide evidence of a dielectric breakdown (arcing) event as the metal ball approaches the electrode (Fig. 1(e) and Movie S3 [20]). The high speed video reveals a brief flash of light located near the closest point of approach. Separate measurements with a photomultiplier tube (PMT) reveal that the light flash is concurrent with a sudden increase in the electrical current flowing through the electrode system (Fig. S8 [20]). Importantly, PMT measurements reveal a similar albeit less intense light flash as a water droplet approaches the electrode (Fig. 4(a,b)). The light flashes were observed every time a ball approached an electrode, but sometimes as low as 48% of the time that a water droplet approached the electrode (Fig. 4(c), cf. Table S1 [20]). It is unclear why a light flash was not observed each time a water droplet approached the electrode; one possibility is that the droplet contacts smaller droplets occasionally left behind on the electrode from previous contacts (Fig. S9 [20]). Our experiments indicate that the number of observed craters is linearly correlated with the number of light flashes detected (Fig. 4(d)), suggesting that a dielectric breakdown event during charge transfer is required for crater formation.

Although similar light flashes have been previously observed when charged objects [13, 14] or liquid drops [26] approached an electrode, recent workers have assumed that electrically bouncing droplets are charged via electrochemical reactions not involving dielectric breakdown [18, 19]. It is known from previous work that application of an arc current on the order of 1-100 amps between stationary electrodes through vacuum can melt the electrodes via Joule heating, with the high pressure present in the plasma jet of the arc pushing the molten material to form micron-scale craters [27, 28]. Our current measurements indicate that the peak current during charge transfer with the water droplets or metal balls is on the order of 10 to 50 nA, i.e., nine orders of magnitude smaller than those previously observed during vacuum arcs that produced craters. Nonetheless, the evidence for dielectric breakdown suggests a similar mechanism is operative despite the tremendously reduced scales in current. The Joule heating associated with the current locally melts the metal electrode, and the expansion of the plasma jet pushes the molten electrode material radially outward. The metal then rapidly cools and re-solidifies, leaving behind the observed craters.

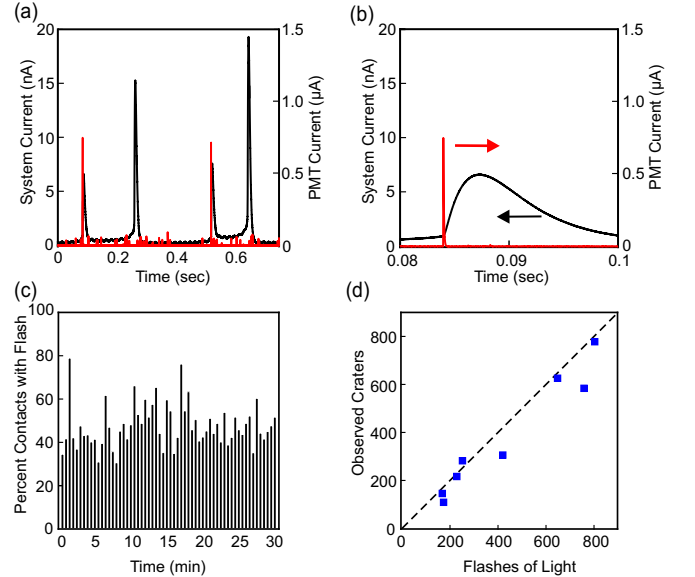The existence of crater formation during charge trans-

FIG. 4. Evidence of dielectric breakdown between a charged water droplet and electrode. (a) The system electrical current (black) and PMT current (red) recorded simultaneously as an aqueous droplet transited between electrodes. Simultaneous peaks in the PMT current and system current occur when the droplet approaches the electrode in view of the PMT. (b) Magnification of the first peak in (a). (c) The percentage of observed charge transfer events when a light flash was also detected by the PMT. Each bar represents 30 seconds of time. (d) Observed number of craters versus extrapolated number of light flashes. The dashed line has a slope of 1. Also see Table S1 [20].

fer has several implications. Fundamentally, the crater formation provides insight on the difficulty of experimentally measuring the amount of charge an object should receive from contact with an electrode, first calculated by Maxwell. Measured charges have fluctuated as high as a factor of three or more from the predicted value [8–15]. The results presented here indicate that the electrodes in those experiments may have undergone morphological changes that affected the charge transfer process; since the craters are not visible to the naked eye, the changes would be difficult to discern. Recently Drews et al. performed experiments and noted variations in the charge acquired by the particle at different electrodes [11]. They speculated that the differences were due to small imperfections on the electrode surfaces that influenced the charge transfer process. The results presented here indicate that the charge transfer process itself creates such imperfections.

Practically, the propensity to form craters might be relevant in the design of lab-on-a-chip devices [17–19], electrowetting devices [16], electrocoalescers [29], printers [30], and other devices [24, 31, 32] that use electrodes to manipulate charged droplets or particles, since repeated crater formation over time might seriously degrade the device. Alternatively, we note that the craters formed here approach sizes as small as 500 nm in diameter, comparable to the wavelength of light. The crater formation thus points to a possible methodology to pattern thin metallic films at dimensions comparable to laser ablation [33] or other photolithographic techniques.

---

* Present Address: Department of Materials Science and Engineering, Massachusetts Institute of Technology, Cambridge, Massachusetts 02139, USA.
† Corresponding Author Email: wdristenpart@ucdavis.edu

[1] J. C. Maxwell, *A Treatise on Electricity and Magnetism*, Vol. 1 (Cambridge University Press, 2010) §175.
[2] J. D. Sartor, J. Meteor. **11**, 91 (1954).
[3] G. M. Panchenkov, V. M. Vinogradov, and V. V. Papko, Chem. Technol. Fuels Oils **6**, 120 (1970).
[4] S. E. Sadek and C. D. Hendricks, Ind. Eng. Chem. Fundam. **13**, 139 (1974).
[5] T. Mochizuki, Y. H. Mori, and N. Kaji, AIChE J. **36**, 1039 (1990).
[6] K. Asano, Am. J. Phys. **43**, 423 (1975).
[7] A. Khayari and A. T. Pérez, IEEE Trans. Dielec. Electr. Insul. **9**, 589 (2002).
[8] A. Y. H. Cho, J. Appl. Phys. **35**, 2561 (1964).
[9] C. R. Knutson, K. V. Edmond, M. T. Tuominen, and A. D. Dinsmore, J. Appl. Phys. **101**, 013706 (2007).
[10] G. M. Colver, J. Appl. Phys. **47**, 4839 (1976).
[11] A. M. Drews, C. A. Cartier, and K. J. M. Bishop, Langmuir **31**, 3808 (2015).
[12] J. B. Olansen, P. F. Dunn, and V. J. Novick, J. Appl. Phys. **66**, 6098 (1989).
[13] S. Birlasekaran, IEEE Trans. Electr. Insul. **26**, 1094 (1991).
[14] R. Tobazéon, J. Phys. D **29**, 2595 (1996).
[15] A. M. Drews, M. Kowalik, and K. J. M. Bishop, J. Appl. Phys. **116**, 074903 (2014).
[16] F. Mugele and J. C. Baret, J. Phys. Condens. Matter **17**, R705 (2005).
[17] D. R. Link, E. Grasland-Mongrain, A. Duri, F. Sarrazin, Z. D. Cheng, G. Cristobal, M. Marquez, and D. A. Weitz, Angew. Chem. Int. **45**, 2556 (2006).
[18] D. J. Im, M. M. Ahn, B. S. Yoo, D. Moon, D. W. Lee, and I. S. Kang, Langmuir **28**, 11656 (2012).
[19] P. Beránek, R. Flittner, V. Hrobař, P. Ethgen, and M. Přibyl, AIP Advances **4**, 067103 (2014).
[20] See Supplemental Material at [URL will be inserted by publisher] for supplemental figures S1-S11, discussion scaling analysis and crater integration, and supplemental movies S1-S4.
[21] H. A. Pohl, *Dielectrophoresis* (Cambridge University Press, 1978).
[22] G. I. Taylor, Proc R. Soc. Lond. A **280**, 383 (1964).
[23] R. T. Collins, K. Sambath, M. T. Harris, and O. A. Basaran, Proc. Natl. Acad. Sci. U.S.A. **110**, 4905 (2013).
[24] Y. M. Jung, H. C. Oh, and I. S. Kang, J. Colloid Interface Sci. **322**, 617 (2008).
[25] A. L. Yarin, Annu. Rev. Fluid Mech. **38**, 159 (2006).
[26] M. Hara, T. Yamashita, and M. Akazaki, J. Electrostat. **13**, 325 (1982).
[27] G. W. McClure, J. Appl. Phys. **45**, 2078 (1974).
[28] B. Jüttner, J. Phys. D **34**, R103 (2001).
[29] S. Mhatre, V. Vivacqua, M. Ghadiri, A. M. Abdullah, M. J. Al-Marri, A. Hassanpour, B. Hewakandamby, B. Azzopardi, and B. Kermani, Chem. Eng. Res. Des. **96**, 177 (2015).
[30] P. Calvert, Chem. Mater. **13**, 3299 (2001).
[31] W. D. Ristenpart, J. C. Bird, A. Belmonte, F. Dollar, and H. A. Stone, Nature **461**, 377 (2009).
[32] B. S. Hamlin, J. C. Creasey, and W. D. Ristenpart, Phys. Rev. Lett. **109**, 094501 (2012).
[33] K. Sugioka and Y. Cheng, Appl. Phys. Rev. **1**, 041303 (2014).